electronic reprint

Acta Crystallographica Section B
Structural Science
ISSN 0108-7681
Editor: **Carolyn P. Brock**

Local and long-range order in ferroelastic lead phosphate at high pressure

R. J. Angel, U. Bismayer and W. G. Marshall

Acta Crystallographica Section B
Structural Science
ISSN 0108-7681

Local and long-range order in ferroelastic lead phosphate at high pressure

R. J. Angel,[a]* U. Bismayer[b] and W. G. Marshall[c]

[a]Crystallography Laboratory, Department of Geological Sciences, Virginia Polytechnic Institute and State University, Blacksburg, Virginia 24060, USA, [b]Mineralogisch Petrographisches Institut der Universitaet Hamburg, Grindelallee 48, D-20146 Hamburg, Germany, and [c]ISIS Facility, Rutherford Appleton Laboratory, Chilton, Didcot, Oxfordshire OX11 0QX, England

Correspondence e-mail: rangel@vt.edu

Received 26 June 2003
Accepted 19 November 2003

Pure lead phosphate, $Pb_3(PO_4)_2$, undergoes a phase transition from $C2/c$ to $R\bar{3}m$ symmetry at a pressure of approximately 1.8 GPa and room temperature. Single-crystal X-ray diffraction measurements of the unit-cell parameters of a sample doped with 1.6% Ba^{2+} for the Pb^{2+} indicates that the doping reduces the transition pressure by approximately 0.1 GPa. The structural evolution of both samples through the phase transition has been determined by Rietveld refinement of neutron powder diffraction data collected to pressures of 6.3 and 3.3 GPa, respectively. There is no evidence for any significant change in the local structure at the phase transition at high pressures; the structure of the $R\bar{3}m$ phase at pressures just above the phase transition includes disordered positions for several atoms. The observation of diffuse scattering from the $R\bar{3}m$ phase at high pressure by single-crystal X-ray diffraction suggests that the disorder is static and arises from the presence of several orientations of the ordered microdomains of the monoclinic local structure. The macroscopic transition from monoclinic to trigonal symmetry therefore appears to correspond to the pressure at which the coherency strains between the locally monoclinic microdomains are sufficient to create a dimensionally trigonal lattice within which local displacements of atoms are still significant. A further pressure increase then decreases the magnitude of these displacements until at 3.5 GPa or higher they are not detectable by our current experimental probes, and the structure appears to have true local and global trigonal symmetry.

1. Introduction

Lead phosphate, $Pb_3(PO_4)_2$, is a model improper ferroelastic material that has been studied extensively by a wide variety of techniques in order to fully characterize its transition behaviour. At ambient conditions $Pb_3(PO_4)_2$ displays $C2/c$ symmetry and at 453 K it transforms to a phase with global $R\bar{3}m$ symmetry. Since the transition is associated with a critical point on the Brillouin zone boundary, the coupling between the symmetry-breaking spontaneous strains arising from the phase transition and the order parameter has to be linear-quadratic, the same as the non-symmetry-breaking strain components. The unusual feature of the phase transition in lead phosphate is that the total spontaneous strain (*ca* 2%) and morphic birefringence (*ca* 2×10^{-2}) at room conditions are unusually large for a phase transition with such second-order coupling between the strain and the order parameters (Wood *et al.*, 1980; Salje *et al.*, 1993). The transition mechanism is related to a shift of the Pb atoms away from the triad axes of

Table 1
Unit-cell parameters of Ba-doped lead phosphate at high pressures as determined by single-crystal X-ray diffraction.

P (GPa)	a (Å)	b (Å)	c (Å)	β (°)	V (Å^3)
10^{-4}	13.8087 (12)	5.6947 (5)	9.4306 (8)	102.367 (7)	724.38 (10)
0.158 (3)	13.8044 (6)	5.6731 (2)	9.4321 (4)	102.467 (3)	721.24 (5)
0.387 (4)	13.7984 (7)	5.6424 (3)	9.4361 (4)	102.603 (4)	716.97 (5)
0.581 (5)	13.7895 (6)	5.6176 (3)	9.4377 (4)	102.688 (3)	713.23 (5)
0.799 (4)	13.7849 (11)	5.5896 (4)	9.4443 (7)	102.819 (6)	709.56 (8)
1.217 (4)	13.7725 (9)	5.5399 (4)	9.4513 (6)	102.994 (5)	702.65 (8)
1.434 (5)	13.7661 (11)	5.5146 (5)	9.4575 (7)	103.082 (6)	699.32 (9)
1.594 (4)	13.767 (3)	5.4954 (10)	9.4674 (17)	103.170 (15)	697.44 (20)
1.729 (5)	13.7702 (11)	5.4730 (4)	9.4764 (6)	103.270 (6)	695.107 (8)
1.734 (5)	5.4713 (3)		20.1009 (7)		521.11 (6)
2.073 (4)	5.4602 (4)		20.0754 (9)		518.33 (7)
2.544 (5)	5.4460 (3)		20.0433 (8)		514.82 (6)
3.260 (6)	5.4273 (3)		19.9973 (6)		510.12 (5)
3.942 (7)	5.4116 (3)		19.9559 (7)		506.12 (5)
4.855 (7)	5.3920 (3)		19.9055 (6)		501.19 (5)

the trigonal phase, together with a correlated tilt of the PO_4 tetrahedra. The transition at high temperature is complicated in the pure material by the persistence of short-range order above the ferroelastic transition, in a regime in which the material is metrically and optically trigonal yet in which 'flip-modes' propagate through the structure (Salje *et al.*, 1983) and the material response to applied mechanical stress appears to reflect domain switching (Cho *et al.*, 2002). The phase transition temperature and the critical behaviour can be modified by doping the material with Ba^{2+} or similar cations (Hensler *et al.*, 1993; Bismayer *et al.*, 1994), which substitute onto the Pb2 site of the structure (Fechtelkord & Bismayer, 1998). At higher levels of doping the dynamic reorientation of the microdomains can be suppressed and at temperatures immediately above the ferroelastic phase transition the material remains macroscopically trigonal, but contains microdomains of lower symmetry that give rise to additional diffuse diffraction maxima (*e.g.* Bismayer & Salje, 1981; Paulmann *et al.*, 1998).

In pure lead phosphate the application of pressure at room temperature leads to the same symmetry change from $C2/c$ to $R\bar{3}m$ at ~1.8 GPa (Decker *et al.*, 1979; Angel & Bismayer, 1999; Angel *et al.*, 2001). The evolution of the spontaneous strain at high pressures indicates that the critical exponent is renormalized to a value close to $\frac{1}{2}$ (Angel & Bismayer, 1999) compared with a value close to $\frac{1}{4}$ for the high-temperature phase transition. In our previous neutron diffraction study we successfully determined the structural evolution of the monoclinic phase up to the phase transition. We found that while one of the symmetrically distinct Pb sites, Pb1, moves towards the symmetry-constrained position which it occupies in the high-symmetry phase, the second Pb2 position does not (Angel *et al.*, 2001). We were also able to collect data from the high-pressure phase in the small range of achievable pressure just above the phase transition. Structure refinements to these data indicate that at 1.93 GPa the Pb2 sites and the O sites are disordered within the trigonal structure. We concluded that the phase transition from $C2/c$ to $R\bar{3}m$ symmetry occurs as a result of the disordering of the displacements at the Pb2 sites and not, to pressures of 1.93 GPa, as the result of the elimination of these displacements (Angel *et al.*, 2001).

We have now extended the previous neutron powder diffraction measurements of pure lead phosphate to higher pressures than previously attained in order to determine whether this structural disorder persists to pressures significantly greater than the phase transition pressure. Measurements of the X-ray diffuse scattering from the paraphase at high pressures provide some further constraints upon the nature of the disorder. These data are supplemented by a similar study of Ba-doped material in order to evaluate the effect of doping upon the high-pressure phase transition.

2. Experimental details

2.1. Sample synthesis

Two samples were used in this study. The pure lead phosphate is the same as that previously used for both a high-pressure single-crystal X-ray diffraction study (Angel & Bismayer, 1999) and a neutron powder diffraction study (Angel *et al.*, 2001). The Ba-doped lead phosphate was synthesized from the starting materials PbO (Merck 7401), $(NH_4)H_2(PO_4)$ (Merck 1126) and $BaCO_3$ (Merck 1713). Pure lead phosphate was first synthesized according to the reaction: $2(NH_4)H_2(PO_4) + 3PbO \rightarrow Pb_3(PO_4)_2 + 3H_2O + 2NH_3$. This material was then powdered, mixed with $BaCO_3$ in proportion to obtain $(Pb_{0.984}Ba_{0.016})_3(PO_4)_2$ and then heated up to 1373 K. Doped crystals were then grown in closed platinum crucibles using the Czochralski technique and the composition was subsequently determined by electron microprobe analysis (Bismayer *et al.*, 1994).

2.2. X-ray diffraction

The evolution of the unit-cell parameters and the equation-of-state of the Ba-doped material were determined by single-crystal X-ray diffraction on a Huber diffractometer driven by the *Single* software (Angel *et al.*, 2000). A 4:1 mixture of methanol:ethanol was used as a hydrostatic pressure medium in an ETH design of a diamond–anvil cell (Miletich *et al.*, 2000). The unit-cell volume of a single crystal of quartz included in the cell was used to determine the pressure of each measurement through its equation-of-state (Angel *et al.*, 1997). Results are listed in Table 1. Note that we use the hexagonal setting for the unit cell of the trigonal phase throughout this paper. The equation-of-state (EoS) of pure lead phosphate was determined previously by the same

methods and using the same pressure scale (Angel & Bismayer, 1999).

The variation of the unit-cell parameters of the trigonal phase of the Ba-doped material with pressure were fitted by linearized versions of the Murnaghan EoS (Angel, 2000) to allow the extrapolation of these unit-cell parameters to pressures below the phase transition and the spontaneous strains arising from the transition to be calculated using these extrapolated values as the reference state. The components of the spontaneous strains were calculated for the choice of Cartesian reference system used by Guimaraes (1979)

$$\begin{aligned} i &// \mathbf{c}_t // (100)_{\rm mono} \\ j &// \mathbf{b}_t // \mathbf{b}_{\rm mono} \\ k &// [210]_t // \mathbf{c}_{\rm mono}. \end{aligned}$$

There are three possible distinct orientations of the monoclinic unit cell with respect to that of the trigonal phase (Fig. 1). The transformation matrices that transform the hexagonal setting of the unit cell to each of these orientations are

$$T1 = \begin{pmatrix} -2/3 & 0 & 2 \\ -1/3 & -1 & 1 \\ 2/3 & 0 & 0 \end{pmatrix},$$

$$T2 = \begin{pmatrix} 1/3 & 1 & -1 \\ -1/3 & 1 & 1 \\ 2/3 & 0 & 0 \end{pmatrix},$$

$$T3 = \begin{pmatrix} 1/3 & -1 & -1 \\ 2/3 & 0 & -2 \\ 2/3 & 0 & 0 \end{pmatrix}.$$

These three matrices are related by the threefold symmetry operator of the trigonal space group. The relationship between the magnitudes of the unit-cell parameters of the monoclinic and hexagonal cell settings can then be derived as

$$\begin{aligned} a &= \left[\frac{a_t^2}{3} + \frac{4c_t^2}{9}\right]^{1/2} \\ b &= a_t \\ c &= 2a_t \cos 30 \\ \beta &= \arctan\left(\frac{c_t}{a_t \cos 30}\right) \\ V &= 4V_t/3, \end{aligned}$$

where a_t and c_t are the values of the unit-cell parameters of the $R\bar{3}m$ phase in the hexagonal setting and symbols without subscripts are the parameters of the monoclinic cell.

The spontaneous strain components arising from the phase transition to the monoclinic phase can be divided into 'symmetry-breaking' and 'non-symmetry-breaking' components as

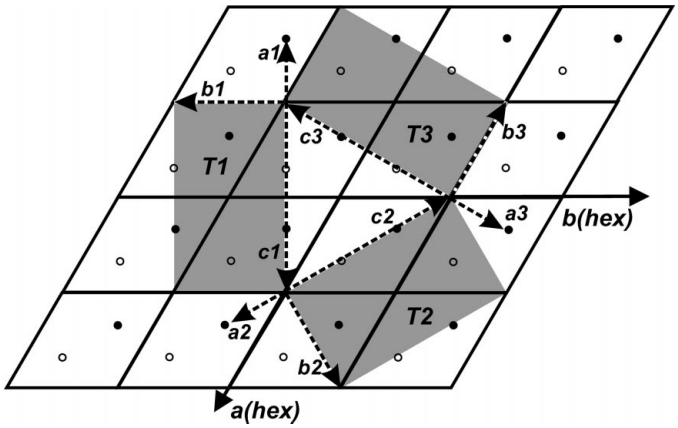

Figure 1
The relationship between the three settings of the monoclinic unit cell with respect to that of the trigonal phase of lead phosphate drawn out on the hexagonal *R* lattice. The circles are lattice points of the *R* lattice; empty circles at z = 1/3, filled circles at z = 2/3. The three shaded rectangles are the (100) faces of the monoclinic cells and are labelled to correspond to the transformation matrices given in the text.

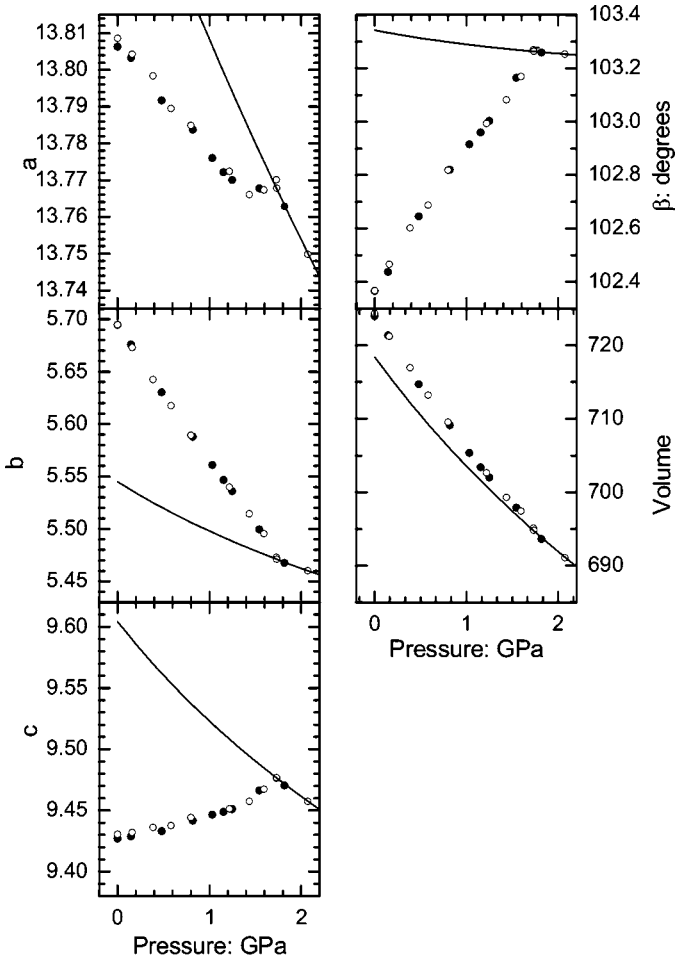

Figure 2
Unit-cell parameters of the pure lead phosphate (Angel & Bismayer, 1999) as solid symbols and Ba-doped material as open symbols, as determined by single-crystal X-ray diffraction. The solid lines are the extrapolation of the trends of the unit-cell parameters of the Ba-doped trigonal phase, transformed to the monoclinic cell setting. Data for the trigonal phase extend to higher pressures than shown (see Table 1). Uncertainties are smaller than the symbol sizes.

$$\varepsilon_{11,\mathrm{nsb}} = 3a\sin\beta/2c_{t0} - 1$$
$$\varepsilon_{22,\mathrm{nsb}} = \varepsilon_{33,\mathrm{nsb}} = (b + c/3^{1/2})/2a_{t0} - 1$$
$$\varepsilon_{13,\mathrm{nsb}} = \varepsilon_{12,\mathrm{nsb}} = \varepsilon_{23,\mathrm{nsb}} = \varepsilon_{12,\mathrm{sb}} = \varepsilon_{23,\mathrm{sb}} = \varepsilon_{11,\mathrm{sb}} = 0$$
$$\varepsilon_{22,\mathrm{sb}} = -\varepsilon_{33,\mathrm{sb}} = (b - c/3^{1/2})/2a_{t0}$$
$$\varepsilon_{13,\mathrm{sb}} = (c + 3a\cos\beta)/4c_{t0},$$

where a_{t0} and c_{t0} are the values of the unit-cell parameters of the $R\bar{3}m$ phase in the hexagonal setting extrapolated to the same pressure at which the monoclinic cell parameters a, b, c and β were measured. The volume strain is simply $V_s = 3V/4V_{t0} - 1$, where V_{t0} is the extrapolated volume of the unit cell of the trigonal phase in the hexagonal setting. Note that the expressions given above reduce to those used by Guimaraes (1979) and by Salje *et al.* (1993) when the non-symmetry-breaking strains arising from the transition are ignored.

Measurements of the diffuse scattering from a single crystal of pure lead phosphate at high pressure were performed with an Xcalibur-2 diffractometer equipped with a conventional Mo X-ray tube, operated at 39 KV (to avoid $\lambda/2$ contamination) and 50 mA, and an Enhance incident beam optic. Data were collected with ω scans of the diamond cell. The individual images obtained on the CCD camera were then transformed and combined by software to produce undistorted images of reciprocal lattice sections. No rescaling of intensities or background subtraction was performed on these data, except that required for detector flood-field normalization and *Lp* corrections.

2.3. Neutron diffraction

High-pressure neutron powder diffraction data were collected on the HiPr instrument of the PEARL beamline at the ISIS facility, Oxfordshire, England. The instrument is a medium-resolution ($\Delta d/d \simeq 0.008$ at $2\theta = 90^\circ$), high-incident flux neutron time-of-flight diffractometer (ISIS Annual Report, 1996). High pressures were generated using a type V3b Paris–Edinburgh cell using standard profile WC/Ni-binder anvils which allow an initial sample volume of $\sim$90 mm^3 (Besson *et al.*, 1992). A 4:1 mixture by volume of deuterated methanol and deuterated ethanol was used as a pressure medium. This mixture remains hydrostatic to at least 6 GPa, but requires the sample to be enclosed in a novel design of gasket in order to prevent the failure of the anvils (Marshall & Francis, 2002). Pressures were determined from the refined unit-cell volumes of the samples through the equations-of-state previously determined by single-crystal X-ray diffraction (this work and Angel & Bismayer, 1999).

Data collection times at each pressure ranged between 2 and 12 h. The diffraction patterns were obtained by electronic focusing of the individual detector element spectra, and normalization of the summed patterns with respect to the incident beam monitor and the scattering from a standard vanadium sample. Corrections were also made for the wavelength and scattering-angle dependence of the neutron attenuation by the anvil (WC) and gasket (TiZr) materials

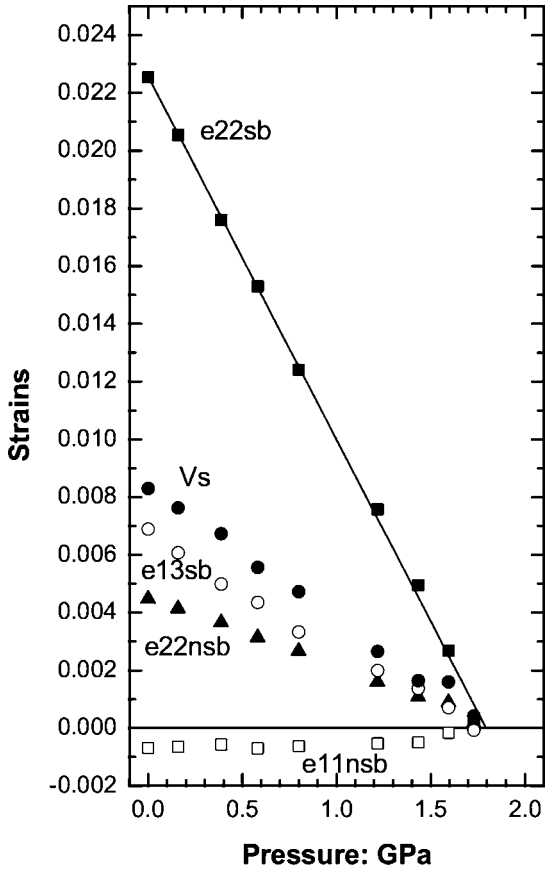

Figure 3
Evolution of the components of the spontaneous strain tensor of Ba-doped lead phosphate calculated on the Cartesian reference system defined by Guimaraes (1979). The line is a linear fit to the component $\epsilon_{22,\mathrm{sb}}$.

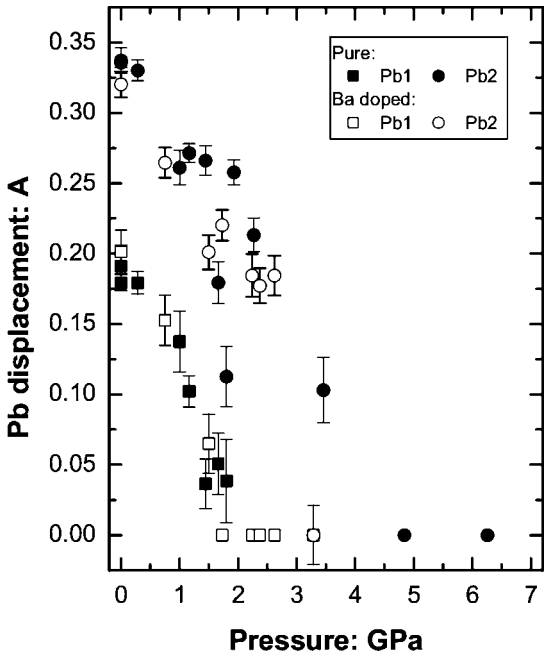

Figure 4
Evolution of the displacement of the Pb1 and Pb2 atoms from the threefold axis of the trigonal unit cell, in both the pure and the Ba-doped lead phosphate.

(Wilson *et al.*, 1995). Rietveld refinements were performed with the *GSAS* program package (Larsen & Von Dreele, 2000) driven by the EXPGUI interface (Toby, 2001) to data with times-of-flight between 2.75 and 17.0 ms, corresponding to *d* spacings between 0.6 and 3.6 Å.

Small portions of some of the diffraction patterns were excluded from the refinement because of the presence of diffraction peaks from additional unidentified minor phases at large *d* spacings. At pressures below 1.2 GPa the peaks of the monoclinic phase of lead phosphate are sufficiently well resolved to allow the stable refinement of the profile parameters. At higher pressures, the evolution of the unit-cell metric towards trigonal symmetry means that pairs of monoclinic peaks are no longer resolved and, as a result, the unit-cell parameters and the profile parameters of the lead phosphate cannot be refined simultaneously. In these cases, the profile parameters were fixed at the refined values obtained from lower pressure datasets; for a given sample loading these parameters did not vary by more than 2 e.s.u.'s between datasets collected at different pressures. The correlation between positional and displacement parameters in the refinement sometimes led to instability or physically unreasonable variations in bond lengths between structures determined at consecutive pressures. In our previous analysis (Angel *et al.*, 2001) we overcame this problem by constraining the displacement parameters to the values determined in a previous single-crystal diffraction experiment. In the current analysis we chose an alternative method of imposing soft constraints on the internal bond lengths and angles of the PO_4 tetrahedron, and by constraining the displacement parameters of chemically equivalent atoms to be the same. Although these constraints only contribute around 1% to the total weighted-chi-squared residual, they are sufficient to stabilize the refinements. We should emphasize that the addition of these soft restraints does not substantially influence the refined positional parameters of the Pb atoms or the Pb—O bond lengths that we discuss below, but, for the sake of consistency, we also include the results of new refinements with these

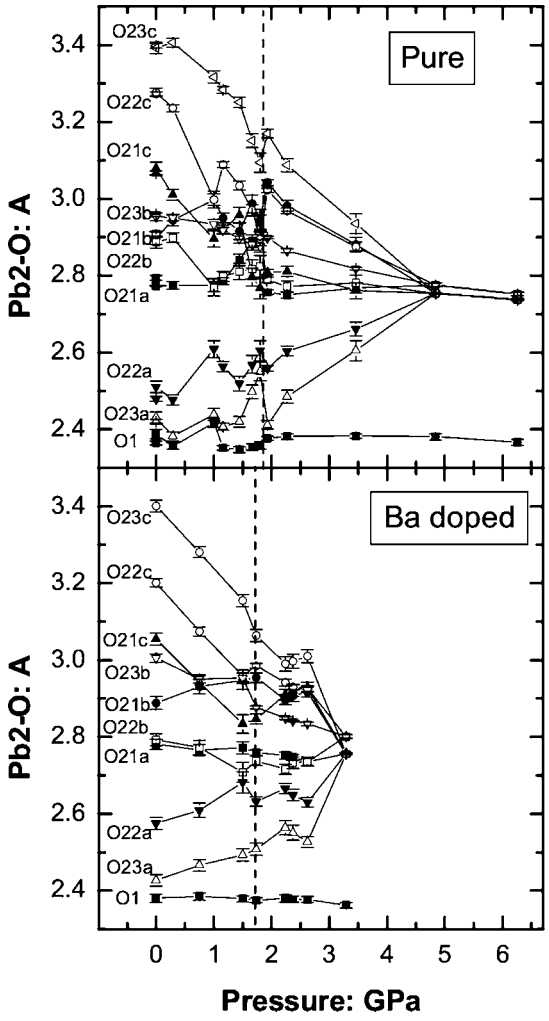

Figure 5
Variation of the individual Pb2—O distances in pure lead phosphate (top) and the Ba-doped material (bottom). The bond lengths in the trigonal phase are calculated for the local configuration shown in Fig. 6(*b*).

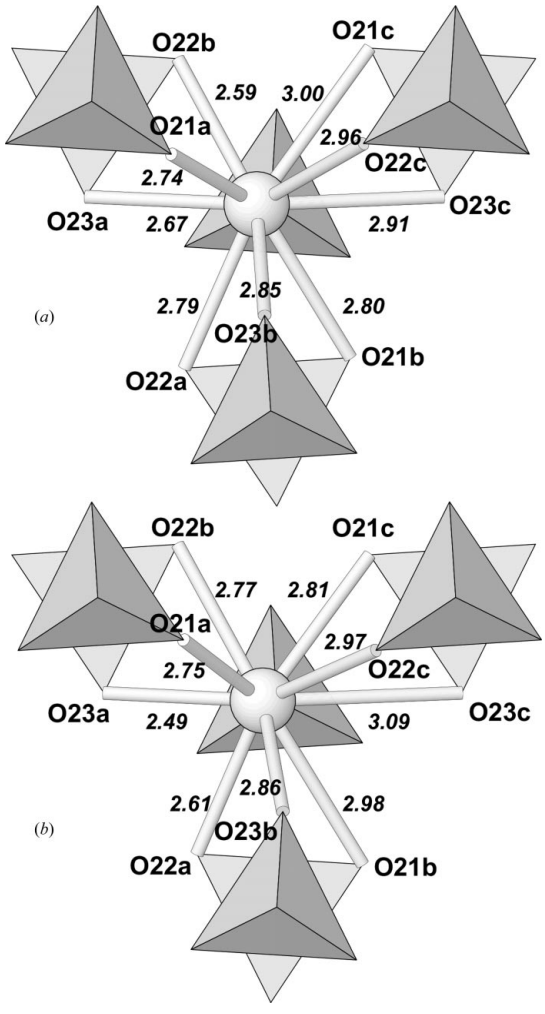

Figure 6
Two possible local configurations for the Pb2 site that can be derived from the split-site models of the trigonal phase of pure lead phosphate at 2.27 GPa (refinement S3P3X0), assuming that the PO_4 tetrahedra remain undistorted. The configuration shown in (*b*) more closely resembles that of the monoclinic phase than that in (*a*). Pb—O bond lengths are given in Å.

Table 2
Refinement models for high-pressure neutron powder diffraction data.

Run + refinement	Pressure (GPa)	Space group	Refinement model	Soft constraints	R_{wp}
Pure lead phosphate					
S2P0	0.000	$C2/c$	Ideal mono with U_{iso}(O) all equal; U_{iso}(Pb1) = U_{iso}(Pb2)	P—O and O—P—O	0.042
S3P1	0.000	$C2/c$	As S2P0	P—O and O—P—O	0.041
S2P6	0.288	$C2/c$	As S2P0	P—O and O—P—O	0.051
S3P2	1.000	$C2/c$	As S2P0	P—O and O—P—O	0.047
S2P12	1.162	$C2/c$	As S2P0	P—O and O—P—O	0.038
S2P14	1.443	$C2/c$	As S2P0	P—O and O—P—O	0.061
S2P16	1.663	$C2/c$	As S2P0 plus profile params = S2P14	P—O and O—P—O	0.064
S2P18	1.804	$C2/c$	As S2P16	P—O and O—P—O	0.082
S2P19D	1.930	$R\bar{3}m$	Pb2 at 0yz; O1 and O2 split; U_{iso}(O1) = U_{iso}(O2); U_{iso}(Pb1) = U_{iso}(Pb2)	P—O	0.044
S3P3X0	2.270	$R\bar{3}m$	Pb2 at 0yz; O2 split; U_{iso}(O1) = U_{iso}(O2); U_{iso}(Pb1) = U_{iso}(Pb2)	None	0.034
S3P4X0	3.460	$R\bar{3}m$	As S3P3X0	None	0.032
S3P5T	4.840	$R\bar{3}m$	Ideal trigonal; U_{iso}(O1) = U_{iso}(O2); U_{iso}(Pb1) = U_{iso}(Pb2)	None	0.043
S3P6T	6.260	$R\bar{3}m$	As S3P5T	None	0.046
Ba-doped lead phosphate					
S4P7	0.0	$C2/c$	Ideal mono with U_{iso}(O) all equal; U_{iso}(Pb1) = U_{iso}(Pb2)	P—O and O—P—O	0.034
S4P12	0.75	$C2/c$	As S4P7	P—O and O—P—O	0.035
S4P19MONO†	1.50	$C2/c$	As S4P7 plus profile parameters = S4P12	P—O and O—P—O	0.035
S4P22‡	1.73	$R\bar{3}m$	Pb2 at 0yz; O1 and O2 split; U_{iso}(O1) = U_{iso}(O2); U_{iso}(Pb1) = U_{iso}(Pb2)	P—O	0.028
S4P29	2.24	$R\bar{3}m$	As S4P22	P–O	0.034
S4P35	2.62	$R\bar{3}m$	As S4P22	P—O	0.036
S4P43	2.37	$R\bar{3}m$	As S4P22	P—O	0.029
S4P55Tiso	3.29	$R\bar{3}m$	Ideal trigonal; U_{iso}(O1) = U_{iso}(O2); U_{iso}(Pb1) = U_{iso}(Pb2)	None	0.044

† S4P19 was first refined in a trigonal space group. The refined peak widths were almost double those of S4P7 and S4P12, indicating that the sample is still monoclinic at this pressure. ‡ S4P22 is very close to the phase transition. Peak widths for the trigonal model are indistinguishable from those at higher pressures, so the reported refinement is trigonal. However, the structure could be just in the monoclinic field with the monoclinic splitting not resolvable.

constraints to the S2 datasets collected previously (Angel *et al.*, 2001). A March–Dollase function with one refinable parameter was used to correct the intensities for the preferred orientation arising from the dominant $(100)_{mono} \equiv (001)_{trig}$ cleavage of the material. The patterns also included diffraction maxima from the WC anvils of the pressure cell and from Ni which is present as a binder in the WC, so the scale, profile and unit-cell parameters of these phases were also refined.

3. Results

3.1. Cell parameters and spontaneous strain

The evolution of the unit-cell parameters of the Ba-doped sample is very similar to that previously determined for the pure material (Fig. 2). Therefore, at pressures significantly below the phase transition the components of the spontaneous strain tensor of the Ba-doped material are very similar to those of the pure material and vary linearly with pressure, indicating that the critical exponent β has a value close to $\frac{1}{2}$ (Fig. 3). Linear extrapolation with pressure of these components to zero suggests that the phase transition pressure would be around 1.8 GPa, essentially identical to that of the pure material. However, the cell parameters determined at 1.734 (5) GPa indicate that the lattice is hexagonal within the estimated uncertainties and no intensity could be detected at the positions of the 021 and $02\bar{1}$ reflections that are the strongest accessible monoclinic reflections to become forbidden in the trigonal phase. Close examination of the variation of the unit-cell parameter a indicates that perhaps more complex behaviour occurs in a pressure interval of ~0.3 GPa below the transition (Fig. 2).

Unconstrained unit-cell parameters of the Ba-doped sample at 1.729 (5) GPa show significant deviations from a hexagonal lattice metric, while the residual intensity is present at the positions of the monoclinic 021 and $02\bar{1}$ reflections. The transition pressure of the Ba-doped sample has therefore been bracketed approximately 0.09 GPa below that of the pure lead phosphate (Angel & Bismayer, 1999). This is consistent with the ~10 K reduction of the critical temperature at room pressure as a result of doping by Ba (Bismayer *et al.*, 1994) and the slope of the phase boundary in P–T space (Midorikawa *et al.*, 1981).

3.2. Structural evolution

Despite renormalization of the critical pressure, the structural evolution of the monoclinic phase of the Ba-doped material is very similar to that of pure lead phosphate. In both materials the degree of internal structural distortion from the high-symmetry trigonal structure decreases continuously with increasing pressure as the symmetrically independent atoms shift towards the symmetry-constrained positions that they would occupy in the trigonal phase. While the displacement of the Pb1 site appears to extrapolate to zero in the neighbourhood of the phase transition, that of the Pb2 site does not (Fig. 4). As a result the Pb2— bond distances in both the pure lead phosphate and the Ba-doped sample still exhibit significant

monoclinic distortion immediately below the ferroelastic transition (Fig. 5).

Above the ferroelastic phase transition both samples are metrically trigonal and the diffraction intensities are consistent with the same space group as found for the high-temperature phase, $R\bar{3}m$. In this space group all the atoms except O2 should occupy special symmetry-constrained positions with coordinates $00z$, while O2 occupies a site with m symmetry at $-xxz$. However, in a pressure interval of approximately 1 GPa above the phase transition in both samples, refinement of the anisotropic displacement parameters leads to values of $U_{11} = U_{22}$ for the Pb2 atom that are significantly larger by a factor of 4–10 than the U_{33} parameter. This indicates that there is either significantly greater thermal motion of the Pb2 site in the xy plane than perpendicular to it or that there is significant positional disorder of the Pb2 sites around the symmetry-constrained position. These diffraction data can be fitted equally well by a split-site model in which the Pb2 atom and, in some cases, the O1 and O2 atoms are allocated to split sites located off the triad axis. In our previous study (Angel *et al.*, 2001) we allocated Pb2 to a site at $-xxz$ in the refinement to our single dataset of the high-pressure phase. However, transformation of the fractional coordinates of the Pb2 sites in the monoclinic phase reveals that the Pb2 site first moves with increasing pressure towards a position equivalent to xyz with $x = 0$ in the hexagonal setting of the unit cell, suggesting that this is a more consistent choice for the split position in the trigonal structure. The quality-of-fit to the data does not distinguish these two choices; they may well be simplistic representations of a more complex distribution of positions within the structure. As pressure is increased further above the phase transition the refined displacement of the Pb2 and O sites from the ideal positions in space group $R\bar{3}m$ becomes smaller. Whenever the refined displacement was less than its e.s.u. we set the atom onto the ideal position in order to obtain the results presented here. Table 2 summarizes the final refinement model used for each data set. The refinement of split positions allows a large number of possible local configurations to be chosen from various combinations of split-atom positions. However, by making the further assumption that the PO_4 tetrahedra remain undeformed we can reduce the possible configurations around the Pb2 site to just two (Fig. 6). One of these (Fig. 6*b*) corresponds to the configuration found in the monoclinic phase and the evolution of Pb2—O bond lengths calculated from this model is continuous across the ferroelastic phase transition (Fig. 5). As pressure is increased further the split sites converge until they are no longer distinguishable from the ideal symmetry-constrained positions of the $R\bar{3}m$ structure.

3.3. Diffuse scattering

The X-ray single-crystal diffraction patterns of the high-pressure ferroelastic phase of pure lead phosphate at 2.0 GPa include very weak diffuse reflections at positions that can be indexed with half-integer indices of the hexagonal setting of the unit cell. In order to understand the origin of this diffuse intensity it is useful to review the origin of similar intensity in other mixed crystals of the same structure type (*e.g.* Bismayer & Salje, 1981; Bismayer *et al.*, 1982; Röwer *et al.*, 1997; Paulmann *et al.*, 1998). As an example Fig. 7 shows three sections of the diffraction pattern of $Pb_3(As_{0.52},P_{0.48})_2O_4$ at room temperature, in which the diffuse intensity is much stronger than observed at high pressures. Under these conditions $Pb_3(As_{0.52},P_{0.48})_2O_4$ has $R\bar{3}m$ symmetry and is in the paraphase (Bismayer & Salje, 1981). The diffraction pattern contains two types of diffraction maxima. The sharp Bragg reflections can be indexed on the hexagonal setting of the unit cell with the R lattice. Around each Bragg reflection is a group of four or six weak and diffuse intensity maxima that can be indexed with half integers in relation to the hexagonal unit cell (Fig. 7). The application of the three transformation matrices listed in §2.2 to the half-integer indices of the diffuse maxima shows that each group of six maxima comprises three pairs of reflections. Each pair corresponds to positions where Bragg maxima from one of the monoclinic unit cells would occur below the phase transition and they exhibit the extinction rules corresponding to the $C2/c$ symmetry of the monoclinic phase. Groups of only four diffuse maxima therefore arise when the positions of the third pair correspond to symmetry-forbidden reflections in one of the three possible monoclinic domain orientations (as shown for the satellites around the 300 reflection shown in Fig. 7). The presence of these diffuse maxima

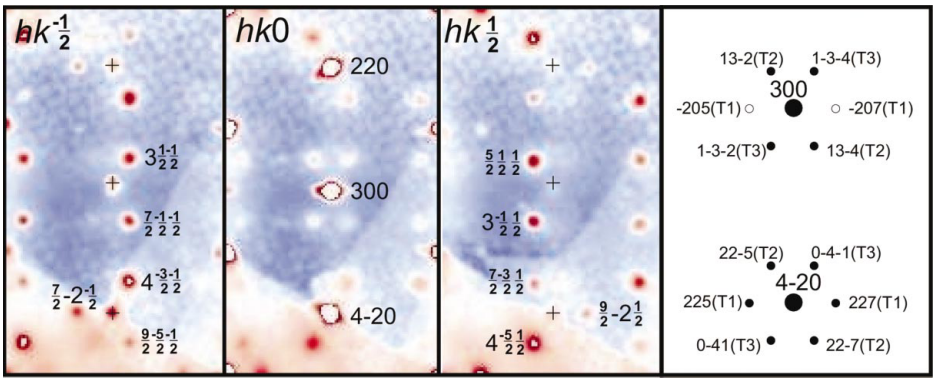

Figure 7
Reciprocal lattice sections $hk\frac{1}{2}$, $hk0$ and $hk\frac{1}{2}$ around the 300 Bragg reflection of the hexagonal setting of the unit cell reconstructed from new CCD data images collected from a single crystal of $Pb_3(As_{0.52},P_{0.48}O_4)_2$ at ambient conditions by X-ray diffraction. Each Bragg peak is surrounded by four or six diffuse satellites that are indexed by half-integer values of h, k and l on the trigonal unit cell. The diagram on the right indicates the indexing with monoclinic indices of two sets of satellites on the unit cells of the three possible domain orientations. Note that the 300_{trig} reflection only has four diffuse satellites because the pair that would correspond to domain T1 is forbidden by the $C2/c$ symmetry of the monoclinic structure. Sample synthesized by Bismayer & Salje (1981).

from the trigonal phase of doped and mixed crystals at room pressure has therefore been interpreted as indicating that the paraphase contains small clusters with local monoclinic structure which, nevertheless, together exhibit an overall hexagonal lattice symmetry. In pure lead phosphate these diffuse reflections arise from the dynamic flip-mode phase (Salje *et al.*, 1983), but in mixed crystals they correspond, at least in part, to static monoclinic clusters (Bismayer *et al.*, 1982; Bismayer *et al.*, 1995).

Fig. 8 shows that the diffuse maxima we have observed in pure lead phosphate at high pressure are much weaker than those observed in $Pb_3(As_{0.52},P_{0.48}O_4)_2$ at ambient conditions. Part of this arises from experimental constraints – the crystal mounted in the diamond–anvil pressure cell is much smaller and the intensity is further reduced by the ~60% absorption by the diamond–anvil cell. Lastly, the diamond anvils contribute a significant structured background including Compton scattering and Bragg reflections. Nonetheless, Fig. 8 shows that a significant intensity is present at the half-integer positions around the Bragg spots 300 and $4\bar{2}0$, as well as their symmetry equivalents (not shown). As far as they can be detected, they appear to exhibit the same extinction rules as we have described for the mixed crystals at ambient conditions. These diffuse reflections were not detected upon pressure increase to 2.5 GPa, but reappeared when pressure was once again reduced to ~2.0 GPa. By analogy with the behaviour of doped crystals such as $Pb_3(As_{0.52},P_{0.48}O_4)_2$ we venture to suggest that the diffuse scattering in pure lead phosphate at high pressures arises from monoclinic clusters that persist within the metrically trigonal phase for a pressure interval of at least 0.2 GPa above the ferroelastic phase transition.

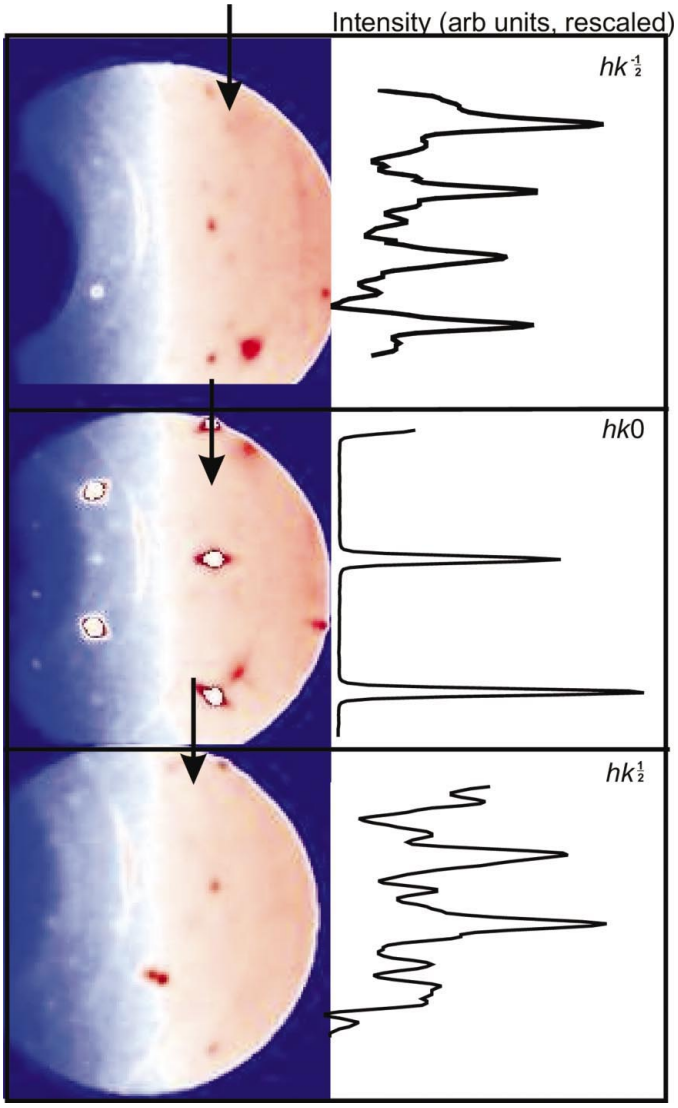

Figure 8
Reciprocal lattice sections $hk\bar{\frac{1}{2}}$, $hk0$ and $hk\frac{1}{2}$ around the 300 Bragg reflection reconstructed from CCD data images collected from a pure lead phosphate single crystal held at 2.0 GPa in a diamond–anvil cell. The layers $hk\frac{1}{2}$ and $hk\frac{1}{2}$ show clear evidence of diffuse reflections at the half-integer positions along the arrowed directions, as shown by the intensity profiles on the right. Note that in addition, the $hk\frac{1}{2}$ and $hk\frac{1}{2}$ layers also exhibit 'spill-over' of the Bragg reflections from the $hk0$ layer. These sections can be compared with the much stronger diffuse scattering displayed in Fig. 7.

4. Summary

The ferroelastic properties of the lead phosphate structure type are dominated by the behaviour of the Pb2 site. Substitution of Ba onto this site tends to suppress the dynamic behaviour observed in the pure material at high temperatures. Therefore, the similarity of the evolution of the paraphase at high pressures in doped and undoped material points to the local disorder at the Pb2 site being static, rather than dynamic, in character. The similarity of the X-ray diffuse scattering from the paraphase just above the transition to that observed in mixed crystals, in which the long-range disorder is known to arise from the presence of statically ordered microdomains, supports this interpretation. Our data therefore show that the ferroelastic transition from monoclinic to trigonal global symmetry does not involve any significant change in the local structural distortions. Instead, the transition pressure appears to correspond to a pressure at which the coherency strains between the locally monoclinic microdomains are sufficient to create a metrically trigonal lattice within which local displacements of Pb2 atoms from the triad axis are still significant. This structure of clusters or microdomains persists in the trigonal phase so that the long-range average structure as determined by neutron powder diffraction appears to include disordered split sites. Further pressure increases then decreases the magnitude of these displacements until at 3.5 GPa or higher they are not detectable by our current experimental probes and the structure appears to have true local and global trigonal symmetry.

X-ray diffuse scattering measurements were performed on an instrument purchased with the support of the NSF grant CHE-0131128. Neutron diffraction experiments were performed on the PEARL beamline of the ISIS facility with the support of the Central Laboratories Research Council

(CLRC) and funded by the UK Engineering and Physical Sciences Research Council (EPSRC). Travel support was provided by BMBF grant 05KS1 GUA/7 and NSF through the COMPRES Neutrons grant (EAR 0135554). The technical assistance of Mr D. J. Francis with the experiments at ISIS, the help of Brian Toby (*NIST*) with the generation of the cif and the comments of two reviewers were greatly appreciated.

References

Angel, R. J. (2000). *Transformation Processes in Minerals*, edited by S. A. T. Redfern & M. A. Carpenter, pp. 85–104. Washington DC: The Mineralogical Society of America.

Angel, R. J., Allan, D. R., Miletich, R. & Finger, L. W. (1997). *J. Appl. Cryst.* **30**, 461–466.

Angel, R. J. & Bismayer, U. (1999). *Acta Cryst.* B**55**, 896–901.

Angel, R. J., Bismayer, U. & Marshall, W. G. (2001). *J. Phys. Condens. Matter*, **13**, 5353–5364.

Angel, R. J., Downs, R. T. & Finger, L. W. (2000). *High-Pressure and High-Temperature Crystal Chemistry*, edited by R. M. Hazen & R. T. Downs, pp. 559–596. Washington DC: The Mineralogical Society of America.

Besson, J. M., Nelmes, R. J., Hamel, G., Loveday, J. S., Weill, G. & Hull, S. (1992). *Physica B*, **180**, 907–910.

Bismayer, U., Hensler, J., Salje, E. & Guttler, B. (1994). *Phase Transit.* **48**, 149–168.

Bismayer, U., Röwer, R. W. & Wruck, B. (1995). *Phase Transit.* **55**, 169–179.

Bismayer, U. & Salje, E. (1981). *Acta Cryst.* A**37**, 145–153.

Bismayer, U., Salje, E. K. H. & Joffrin, C. (1982). *J. Phys.* **43**, 1379–1388.

Cho, Y. C., Lee, H. J., Park, S. E., Cho, C. R. & Jeong, S. Y. (2002). *Phys. Rev. B*, **66**, No. 184103.

Decker, D. L., Petersen, S., Debray, D. & Lambert, M. (1979). *Phys. Rev. B*, **19**, 3552–3555.

Fechtelkord, M. & Bismayer, U. (1998). *Solid State Nucl. Magn. Reson.* **11**, 231–241.

Guimaraes, D. M. C. (1979). *Phase Transit.* **1**, 143–154.

Hensler, J., Boysen, H., Bismayer, U. & Vogt, T. (1993). *Z. Kristallogr.* **206**, 213–231.

ISIS Annual Report (1996). Dedicated Facility for High Pressure Diffraction. Rutherford Appleton Laboratory Report TR-96-050, 61–62.

Larsen, A. C. & Von Dreele, R. (2000). *GSAS*. Los Alamos National Laboratory, New Mexico, USA.

Marshall, W. G. & Francis, D. J. (2002). *J. Appl. Cryst.* **35**, 122–125.

Midorikawa, M., Kashida, H. & Ishibashi, Y. (1981). *J. Phys. Soc. Jpn*, **50**, 1592–1594.

Miletich, R., Allan, D. R. & Kuhs, W. F. (2000). *High-Pressure and High-Temperature Crystal Chemistry*, edited by R. M. Hazen & R. T. Downs, pp. 445–519. Washington DC: The Mineralogical Society of America.

Paulmann, C., Bismayer, U. & Aroyo, M. (1998). *Phase Transit.* **67**, 1–26.

Röwer, R. W., Bismayer, U., Morgenroth, W. & Guttler, B. (1997). *Solid State Ion.* **101**, 585–589.

Salje, E., Devarajan, V., Bismayer, U. & Guimaraes, D. M. C. (1983). *J. Phys. C: Solid State Phys.* **16**, 5233–5243.

Salje, E. K. H., Graeme-Barber, A., Carpenter, M. A. & Bismayer, U. (1993). *Acta Cryst.* B**49**, 387–392.

Toby, B. H. (2001). *J. Appl. Cryst.* **34**, 210–213.

Wilson, R. M., Loveday, J. S., Nelmes, R. J., Klotz, S. & Marshall, W. G. (1995). *Nucl. Instrum. Methods A*, **354** 145–148.

Wood, I. G., Wadhawan, V. K. & Glazer, A. M. (1980). *J. Phys. C: Solid State Phys.* **13**, 5155–5164.